ELSEVIER

Thin Solid Films 360 (2000) 139–144

thin solid films

www.elsevier.com/locate/tsf

Near-field microscopy of collapsed Langmuir–Blodgett films

Steven R. Cordero, Kenneth D. Weston, Steven K. Buratto*

Department of Chemistry, University of California, Santa Barbara, CA 93106-9510, USA

Received 21 June 1999; received in revised form 1 October 1999; accepted 22 October 1999

Abstract

Fluorescence near-field scanning optical microscopy (FL-NSOM) is used to probe the nanoscale structure in stained phospholipid monolayers deposited on glass substrates at moderate surface pressures. The FL-NSOM images reveal new liquid-expanded (LE) and liquid-condensed (LC) domains, including one-to-one correlation between fluorescence contrast and film topography. In particular, films of the phospholipid DPPC stained with $DiIC_{12}$ exhibit multilayer structures that are observed within the solid phase domains and have LE-like fluorescence signals. These features are attributed to clusters of dye molecules resulting from the localized collapse of the film upon compression. Such collapsed features are also observed in supported films of 100% $DiIC_{12}$ deposited at high surface pressure. In these films, spatially-resolved spectroscopy shows that the collapsed structures are amorphous based on the fluorescence spectrum while the molecules within the solid phase of the film have a fluorescence spectrum indicative of molecular aggregates.

Keywords: Langmuir–Blodgett films; Fluorescence near-field scanning optical microscopy; $DiIC_{12}$; Liquid-expanded domains; Liquid-condensed domains

1. Introduction

The self-organization properties of amphiphillic molecules at the air–water interface and subsequent transfer to solid supports (Langmuir–Blodgett or Langmuir–Schaeffer transfer) has been widely exploited as a means for organizing molecules in layered structures with applications in biology (synthetic membranes), chemistry (substrates for sensors) and physics (non-linear optics) [1–5]. Local characterization of the resulting monolayer and multilayer films has traditionally relied on far-field microscopy techniques such as Brewster angle microscopy of unstained monolayers and fluorescence microscopy of stained monolayers [6–8]. While these methods have yielded important insights into the microscopic structure of LB films, the spatial resolution of these techniques is limited to several hundred nm by diffraction. Recently, applications of fluorescence near-field scanning optical microscopy (FL-NSOM) [9,10] to LB-films has demonstrated spatial resolution below 50 nm [11,12]. These initial FL-NSOM images have shown the existence of unforeseen nanoscale liquid-expanded (LE) and liquid-condensed (LC) domains, grain boundaries between coalesced LC domains and mixed domains. In addition, the feedback mechanism that regulates the height of the NSOM tip provides a topography signature of the solid (LC) and liquid (LE) domains that can be correlated with the fluorescence signal [12]. Thus, NSOM not only provides high spatial resolution, but also provides a one-to-one mapping of fluorescence and topography simultaneously. In this paper, we use fluorescence NSOM to compare the nanoscale structure of DPPC monolayers supported on glass substrates and stained with two different dye molecules, $DiIC_{12}$ and Bodipy-PC. In each system the dye molecules phase-separate into the LE phase of the monolayer making the LE phase fluorescent while the LC phase is dark. As will be discussed thoroughly in the text, the DPPC/$DiIC_{12}$ films show circular domains of bright fluorescence within solid phase domains that exhibit a corresponding topography feature indicating that the film has collapsed. The DPPC/Bodipy-PC monolayers do not show collapsed structures under the same deposition conditions and show the same nanoscale features seen in previous NSOM experiments.

2. Experimental

The monolayer films utilized in this experiment were assembled at the air–water interface using either a commercial Langmuir trough (Nima, UK) or a home-built Langmuir trough [13]. The phospholipid DPPC (Avanti Polar Lipids, Alabaster, AL) and the fluorescent probes BodipyPC and

* Corresponding author. Tel.: +!-805-893-3393, fax: +1-805-893-4120.
E-mail address: buratto@chem.ucsb.edu (S.K. Buratto)

0040-6090/00/$ - see front matter
PII: S0040-6090(99)00890-1

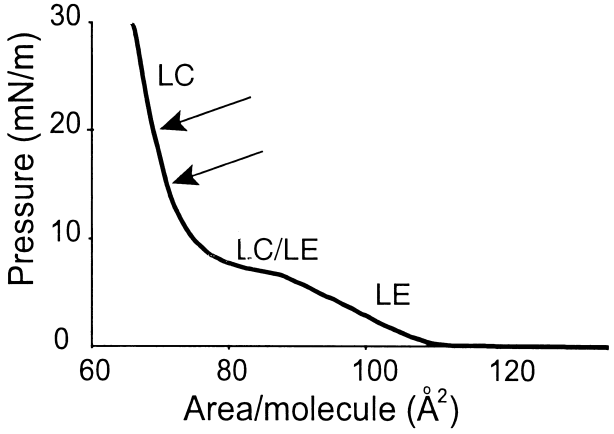

Fig. 1. Typical pressure-area isotherm of DPPC spread on an ultra pure water subphase at room temperature. The different phases are labeled: LE, liquid expanded; LC/LE, liquid condensed/liquid expanded coexistence; and LC, liquid condensed. The LE/LC phase coexistence is evident as observed from the plateau in the isotherm. The monolayer of DPPC/Bodipy-PC was transferred at the point marked by the lower arrow (15 mN/m), and those of both DPPC/$DiIC_{12}$ and pure $DiIC_{12}$ were transferred at the upper arrow (20 mN/m). It should be noted that the small amount of dye added does not adversely affect the phase behavior of DPPC [7].

$DiIC_{12}$ (Molecular Probes, Eugene, OR) were each used as purchased (purity $>$ 99%). The water subphase consisted of ultrapure, deionized (18 MΩ) water (Nanopure System). The stock solution consisted of 1 mM DPPC in chloroform doped with dye in a mole ratio of 100:2 (mol DPPC/mol dye). The stock solution was sonicated for 15 min prior to deposition on the water subphase. Monolayer films were deposited on the subphase by addition of 25 μl of stock solution. The chloroform solvent was then allowed to evaporate for several min before compressing the film. The monolayers were compressed at room temperature with a typical pressure–area isotherm presented in Fig. 1. The initial non-zero slope is indicative of the LE phase followed by the plateau, which represents the phase coexistence of LE/LC. The rise in slope after the coexistence indicates the LC phase. Film fluorescence was recorded in-situ, during compression on the home-built trough, using a microscopy apparatus described previously [13]. Transfer onto 0.17 μm thick glass cover slips was done by either standard vertical deposition on the up-stroke (10 mm/min), or a method analogous to the Schaefer technique. In this technique the substrate is pre-positioned parallel to and just under the surface of the water. Upon removal of a small increment of water from the trough, the monolayer film is laid to rest on the substrate. The deposited monolayer is then observed with far-field fluorescence microscopy to verify that it did not deform during deposition.

Far field fluorescence images are taken using a Leitz fluorescent microscope (Leica Microsystems, Germany) coupled with a CCD camera (Santa Barbara Instrument Group, Santa Barbara, CA). The microscope utilizes reflection geometry along with an interchangeable filter cube system. The filter cubes include a bandpass filter for excitation, a beam splitter for directing both excitation and fluorescence, and a long pass filter for removing the excitation light. In this configuration, filter sets can be easily exchanged to suit the varying fluorescence properties of probe species. The illumination source is a xenon arc lamp, and both the excitation and fluorescence collection are achieved using a 10× objective ($NA = 0.4$).

An NSOM instrument similar to the one shown in Fig. 2 has been described in detail elsewhere [10], and will be only briefly described here. The high optical resolution of NSOM is achieved by the use of a standard tapered optical fiber coated on the side with ~100 nm of Ag to form a sub-wavelength aperture at the tip [9,10]. The optical fiber probes used in the experiments described here all have aperture diameters of 100±10 nm. In transmission NSOM, the sample is excited in the near-field by the sub-wavelength aperture, and the resulting fluorescence is collected in the far-field on the opposite side of the sample with a high NA aperture air objective ($NA = 0.80$). The excitation source was the 514 nm line of an Ar^+ laser (Spectra Physics, Mountain View, CA). The light collected by the objective is passed through a holographic notch filter to remove transmitted laser light. The resulting fluorescence signal is then split 50/50 by a di-chroic beam splitter and sent simultaneously to both a CCD spectrometer (Princeton Inst., Trenton, NJ) and an avalanche photodiode single photon counting module (EG&G, Oak Ridge, TN). This enables the parallel processing of spatially-resolved spectroscopy and integrated fluorescence microscopy. The NSOM scanner is entirely home-built and uses commercial scanning

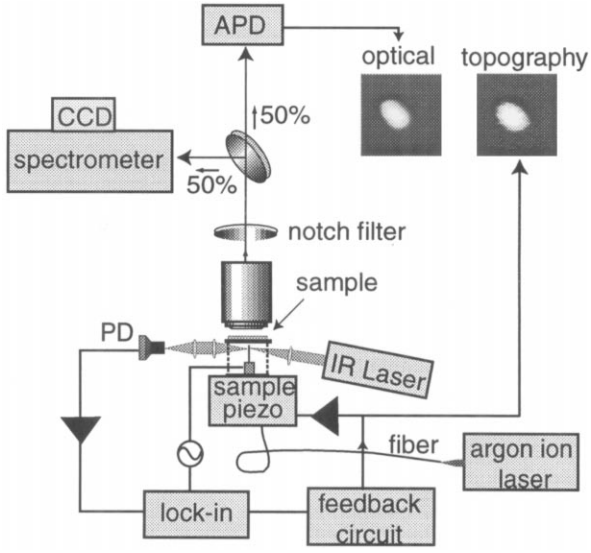

Fig. 2. Block diagram illustrating our transmission NSOM apparatus. The IR laser and the photodiode (PD) are used for the optical shear force detection, which in turn is used in a feedback circuit to maintain the tip in the near-field of the sample as the sample is raster scanned. Transmitted fluorescence is collected in the far-field with a microscope objective, properly filtered, and sent simultaneously to both an avalanche photodiode (APD) and a CCD spectrometer.

electronics (Digital Instruments, Santa Barbara, CA) to raster the sample and form the image.

The NSOM tip aperture is maintained in the near field of the sample surface (10–50 nm) using the standard optically detected shear force feedback technique [14]. The probe is dithered on resonance in the plane of the sample. The dither motion is monitored by focusing laser light normal to the tip surface and detecting the scattered light synchronously with the dither frequency using a lock-in amplifier. As the tip approaches the sample surface, the dither amplitude drops sharply with the tip-sample distance. The output of the lock-in amplifier serves as the input to feedback electronics, which control the tip–sample gap. Upon scanning the sample, the feedback signal provides a topographical map of the sample surface simultaneously with fluorescence. It is important to note that damage to the monolayer film by the shear force feedback was rare and topography features as small as 1 nm (in height) could easily be observed in our experiments.

The same instrumentation shown in Fig. 2 is also adaptable to laser scanning confocal microscopy (LSCM) for images that do not require the high resolution imaging or simultaneous topography imaging of NSOM. In LSCM, the NSOM tip is removed from the apparatus and the laser is directed into the objective and focused to a small spot (~500 nm). The fluorescence is collected with the same objective and detected in exactly the same manner as in fluorescence NSOM. Just as in FL-NSOM an image is formed point-by-point by raster scanning the sample.

3. Results and discussion

The images of Fig. 3 illustrate the advantages in spatial resolution afforded by FL-NSOM over far-field fluorescence microscopy for a DPPC/BodipyPC monolayer deposited in the region of coexistence of the LE and LC phases (see Fig. 3). The image of Fig. 3a shows the characteristic cloverleaf LC domains (dark regions) surrounded by LE domains (bright regions) [6,7]. The LSCM image of Fig. 3b shows a close-up of one of the LC domains of Fig. 3a. This image shows sub-micrometer features not resolved by the FFM technique. Further enhancement of the resolution can be seen in the NSOM images (Fig. 3c) of another finger region of the same monolayer, in which optical resolution of the order of 100 nm was observed. It should be noted that the topography image acquired simultaneously with the NSOM image showed no topography features above the noise of the shear force signal (~1 nm). The very thin (~100 nm) dark lines and bright lines are indicative of grain boundaries in between two LE domains and two LC domains, respectively. The observation of such grain boundaries has proven difficult for far-field techniques but is easily observed in NSOM images of stained phospholipid monolayers [11,12].

Although the topography image of the DPPC/Bodipy-PC monolayer was featureless, the correlation between topogra-

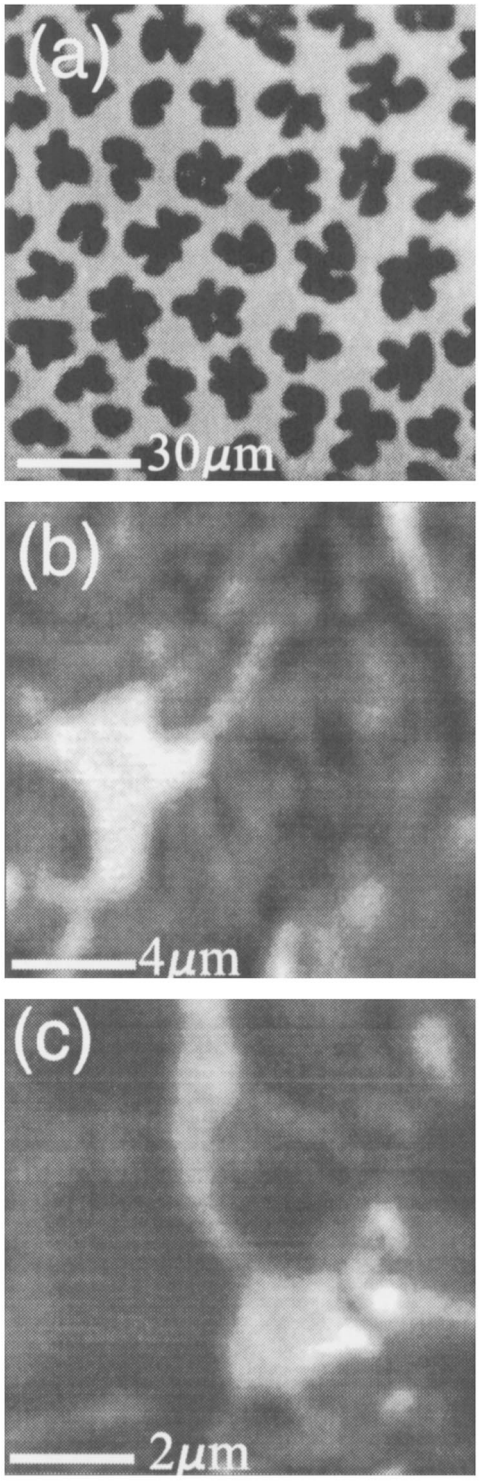

Fig. 3. Fluorescence images of DPPC/BodipyPC monolayers taken with three separate techniques: (a), FFM; (b), LSCM; and (c), NSOM. The neat image captured using FFM has optical resolution on the order of 1 μm. Using LSCM the resolution is narrowed to just under 500 nm, revealing a more complex LC domain than observed using FFM. Resolution less than the diffraction limit (~100 nm) is obtained using NSOM, which reveals a much sharper image than LSCM along with nanoscale features not observed by previous techniques.

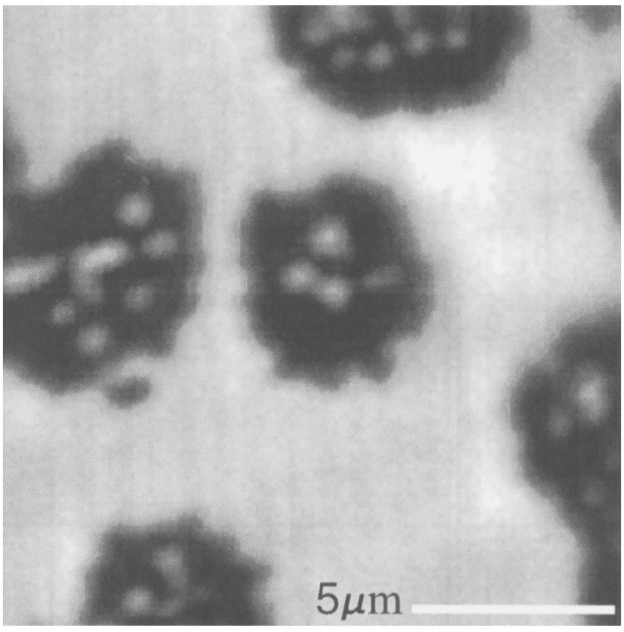

Fig. 4. Fluorescence image of a DPPC/$DiIC_{12}$ monolayer taken with LSCM. The monolayer was transferred at 20 mN/m and room temperature. The LC domains appear to have a honeycomb-type matrix, which could be attributed to small LE domains imbedded in the LC domains.

phy and fluorescence has proven to be an important advantage of NSOM and its application to organic films [12,15,16]. An example of this advantage is illustrated in the images of Figs. 4 and 5. The fluorescence microscopy image of Fig. 4 is from a monolayer film of DPPC/$DiIC_{12}$ transferred at a surface pressure of 20 mN/m (the LC phase region as seen from Fig. 1). The same LC and LE domains seen in the image of Fig. 3a are visible here with an added feature of small circular bright spots within the larger LC domains. A close-up view within one of these LC domains is shown in Fig. 5a. Without further study we might have concluded that these were LE domains embedded in the LC phase based on their LE-like fluorescence signal. However, our NSOM data (Fig. 5a,b) collected from the same sample revealed that there is in fact a one-to-one correspondence between these fluorescent domains and topographical features. A line trace through the topography features shows that the height is of the order 100 nm tall (~75 molecular lengths). We attribute the topographical features to the ultimate collapse of regions concentrated with $DiIC_{12}$ molecules for the following reason. The $DiIC_{12}$ molecules are poorly solvated by the DPPC [17] even in the LE phase, due to the large head group of $DiIC_{12}$ and the alkane chain length mismatch of DiC_{12} (12 carbons) and DPPC (18 carbons). The $DiIC_{12}$ molecules form concentrated regions within the liquid phase of the monolayer, and upon further compression, these regions collapse out of the monolayer structure in order to avoid close packing into the LC phase. Also, the large collapsed structures resemble mountains as is expected from collapsed films [18]. Clustering effects of short chain indocarbocyanine dye molecules in DPPC monolayers have been observed in far-field fluorescence quenching experiments [19]. In addition, these collapsed features were not observed in NSOM images of DPPC/

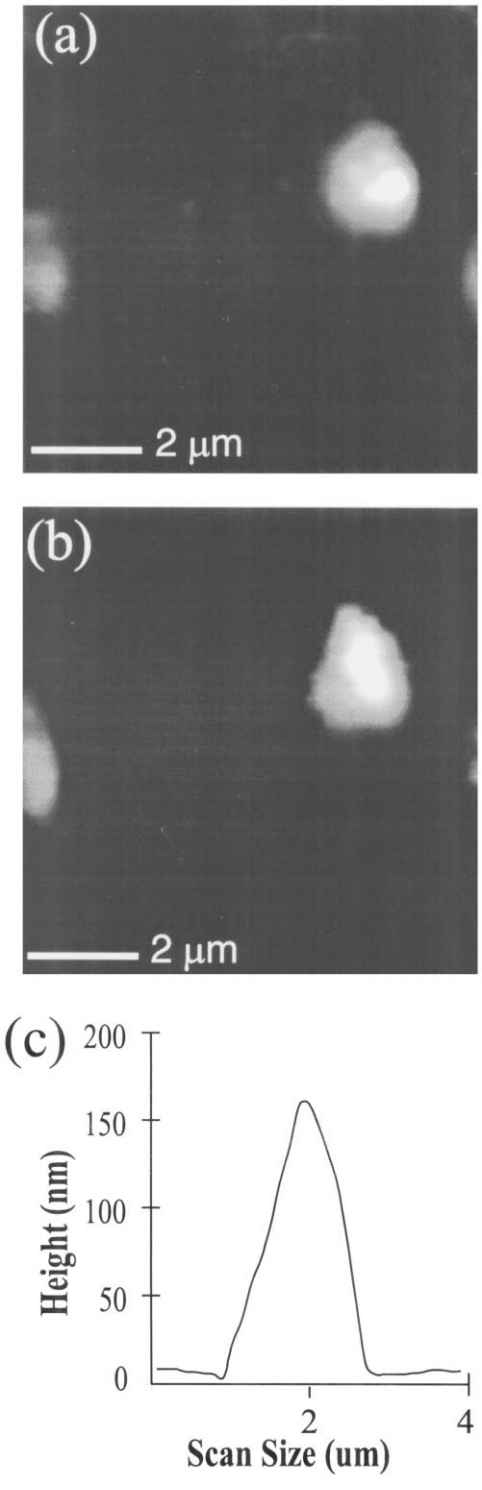

Fig. 5. High resolution fluorescence microscopy of DPPC/$DiIC_{12}$ monolayers. The images in parts (a) and (b) are the FL-NSOM and topography images of two bright spots, respectively. The fluorescence intensity contrast scales linearly from 50 to 200 Kcps. Part (c) shows a line trace through the topography of one of the collapsed structures.

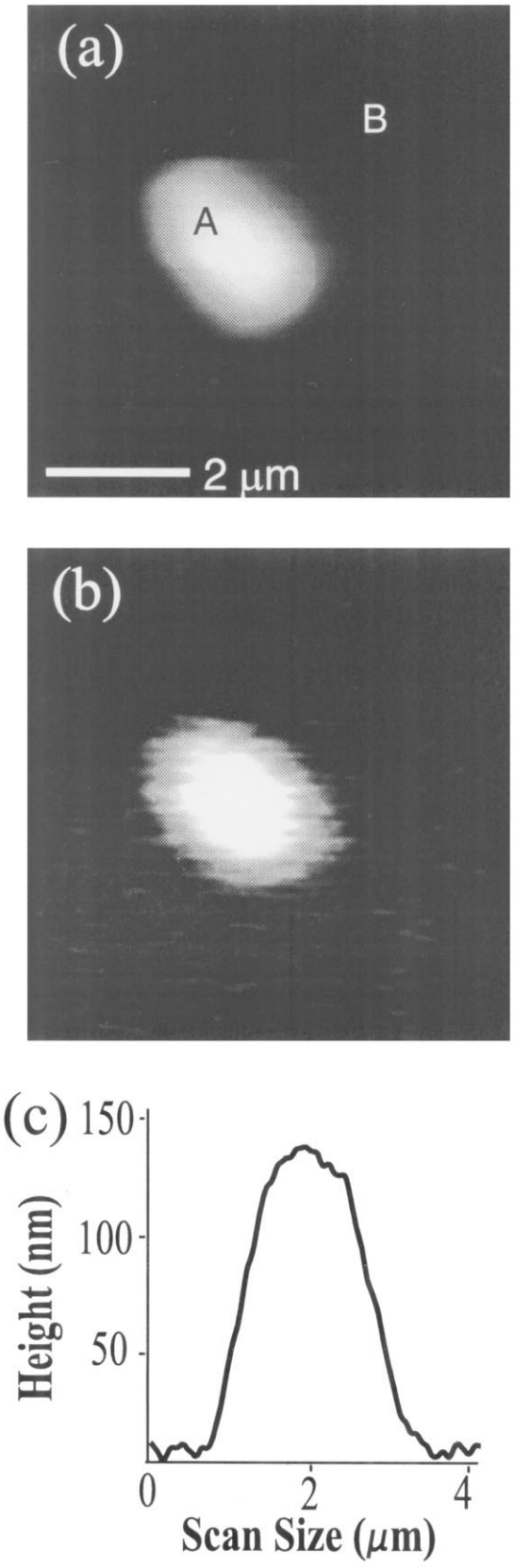

Fig. 6. (a) Simultaneous FL-NSOM; and (b), topography images of single a component $DiIC_{12}$ monolayer. Part (c) shows a line trace through the topography feature in the image of part (b).

$DiIC_{18}$ films (not shown) where the alkane chain length is matched between DPPC and $DiIC_{18}$.

Similarly shaped collapsed features are observed in single component monolayers of $DiIC_{12}$ (1.0 mM solution in chloroform) deposited at a surface pressure above 30 mN/m. In addition, the density of these features increases with increasing surface pressure. Since there is no DPPC present in these films the collapsed features are attributed to a conventional collapse: a release of compression strain for molecules in the crystalline phase at high surface pressure [6–8]. It is important to note that while the mechanism for forming these collapsed features in single component monolayers is different to that in stained phospholipid monolayers, the sizes and shapes of the features are very similar. In the single component monolayers it was possible to use NSOM to probe the internal structure of these collapsed features using spatially-resolved spectroscopy. Also, the heights of the collapsed regions appear to have the same range of sizes as the DPPC/$DiIC_{12}$ films (see Fig. 6c). The absence of a phospholipid in this film makes it optically interesting, because the entire film is fluorescent. The two spectra shown in Fig. 7a were acquired from a bright area (denoted A) and a dim area (denoted B) of the film. It is clear from the spectroscopy data that the dark region is actually emitting, but with a much less intensity (a factor of 10) than the bright domain. As seen in the data of Fig. 7a, the spectra also differ in line-width and relative intensity of the vibronic bands. The differences in the two spectra were studied further by fitting each of the spectra to three gaussians, and then directly comparing the individual gaussians to one another. This analysis showed that the center of mass of spectrum B is shifted 3 nm to the red relative to the spectrum taken from region A. Also, the first vibronic peak of spectrum B became less intense than the second and third vibronic peaks by a factor of two when compared to spectrum A. The spectra taken from the bright domain are identical in shape to that of a thick amorphous film of $DiIC_{12}$ (Fig. 7b). We also observed the same fluorescence spectrum for the collapsed features in the DPPC/$DiIC_{12}$ monolayers. These results imply that the collapsed domains are amorphous and not ordered. On the other hand, the spectra taken from the dark region are indicative of an ordered monolayer film based on the decreased emission, broadened line-shape and a red shift in the peak intensity. All of these are characteristic of aggregate states (such as J- or H-aggregates) common in ordered films of isocyanine dyes such as $DiIC_{12}$ [15,20,21].

4. Conclusion

From our results, we attribute the circular bright regions of the DPPC/$DiIC_{12}$ and single component $DiIC_{12}$ films to amorphous clusters of dye molecules formed from a localized collapse of the Langmuir monolayer. Since these regions make up less than 1% of the surface area of the

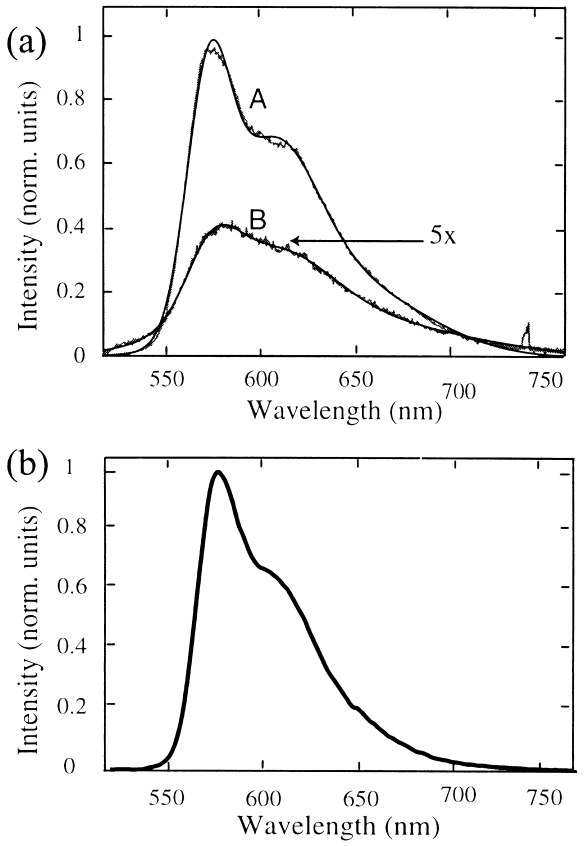

Fig. 7. Fluorescence spectra of a single component $DiIC_{12}$ (a), monolayer; and (b), multilayer taken with NSOM apparatus. The two spectra of part (a) represent spectra taken from spots labeled A and B in the image of Fig. 6a. Also shown in part (a) are the curve fits (bold lines). The spectrum labeled B has been multiplied by a factor of five in order to display both spectra on the same intensity scale. The spectrum in (b) is from a thick amorphous film of $DiIC_{12}$.

film (see Fig. 4), the signature of collapse (leveling off or drop in surface pressure) is often not observed in the isotherm. Furthermore, without the simultaneous topography and fluorescence capability of NSOM, these regions of the film would be nearly impossible to assign. Thus, NSOM techniques represent an important tool in probing nanoscale properties in thin films.

Acknowledgements

The authors acknowledge Dr. Mike Lipp and Prof. Joseph Zasazdinsky from the UCSB Chemical Engineering Department for the preparation of samples and helpful discussions. We also acknowledge Dr. Paul Carson for assistance in fitting our spectra. SKB acknowledges the David and Lucile Packard Foundation (Packard Fellowship) and the Alfred P. Sloan Foundation (Sloan Fellowship). This work was also supported by the NSF (CHE-9501773).

References

[1] G. Decher, F. Klinkhammer, I.R. Peterson, R. Steitz, Thin Solid Films 178 (1989) 445.
[2] M.M. Lipp, K.Y.C. Lee, J.A. Zasadzinski, A.J. Waring, Chemtech 27 (1997) 42.
[3] X. Peng, Y. Zhang, J. Yang, B. Zou, L. Xiao, T. Li, J. Phys. Chem. 96 (1992) 3412.
[4] E.S. Smotkin, C. Lee, A.J. Bard, et al., Chem. Phys. Lett. 152 (1988) 265.
[5] X.K. Zhao, J.H. Fendler, J. Chem. Mater. 3 (1991) 168.
[6] H.M. McConnell, Annu. Rev. Phys. Chem. 42 (1991) 171.
[7] H. Mohwald, Annu. Rev. Phys. Chem. 41 (1990) 441.
[8] M.M. Lipp, K.Y.C. Lee, A. Waring, J.A. Zasadzinski, Biophys. J. 72 (1997) 2783.
[9] E. Betzig, J.K. Trautman, Science 257 (1992) 189.
[10] S.K. Buratto, Curr. Opin. Solid State Mater. Sci. 1 (1996) 485.
[11] J. Hwang, L.K. Tamm, C. Bohm, T.S. Ramalingam, E. Betzig, M. Edidin, Science 270 (1995) 610.
[12] C.W. Hollars, R.C. Dunn, J. Phys. Chem. B 101 (1997) 6313.
[13] M.M. Lipp, K.Y.C. Lee, J.A. Zasadzinski, A.J. Waring, Science 273 (1996) 1196.
[14] E. Betzig, P.L. Finnn, J.S. Weiner, Appl. Phys. Lett. 60 (1992) 2484.
[15] D.A.V. Bout, J. Kerimo, D.A. Higgins, P.F. Barbara, Accounts Chem. Res. 30 (1996) 204.
[16] K.D. Weston, S.K. Buratto, J. Phys. Chem. B 101 (1997) 5684.
[17] R.D. Klausner, D.E. Wolf, Biochemistry 19 (1980) 6199.
[18] Z. Lu, B. Zang, Z. Ai, J. Huang, H. Nakahara, Thin Solid Films 285 (1996) 127.
[19] C.H. Spink, M.D. Yeager, G.W. Feigenson, Biochim. Biophys. Acta 1023 (1990) 25.
[20] M. Vacha, M. Furuki, T. Tani, J. Phys. Chem. B 102 (1998) 1916.
[21] N.C. Maiti, S. Mazumdar, N. Periasamy, J. Phys. Chem. B 102 (1998) 1528.